The Apparent Stratification at the Top of Earth's Liquid Core

Jon Mound*[1], Chris Davies[1], Sebastian Rost[1] & Jon Aurnou[2]

[1] *School of Earth and Environment, University of Leeds, Leeds LS2 9JT, UK*

[2] *Department of Earth and Space Sciences, University of California, Los Angeles, California 90095-1567, USA.*

Earth's magnetic field is generated by turbulent motion in its fluid outer core. Although the bulk of the outer core is vigorously convecting and well-mixed, some seismic, geomagnetic, and geodynamic evidence suggests that a global stably stratified layer exists at the top of Earth's core. Such a layer would strongly influence thermal, chemical, and momentum exchange across the core-mantle boundary (CMB) and thus have significant implications for the dynamics and evolution of the core. However, the existence of thick and strong global stratification is incompatible with the radial motions near the top of the core that are believed necessary to explain observed high-latitude magnetic flux concentrations and patches of reversed magnetic flux. Here we argue that the relevant scenario is not a global layer but regional stratification arising from the lateral variations in CMB heat flux. Based on our extensive suite of numerical simulations we expect that regional thermal inversion layers extend 100's of kilometres into the core under anomalously hot regions of the lowermost mantle. Sufficiently large and strong regional anomalies will dominate the average radial temperature profile and could be mistaken for a globally stratified layer. Dynamic links be-

tween regions of thermal inversion and active convection result in radial motion everywhere within the core, thereby avoiding any conflict with geomagnetic observations.

There is little doubt that the bulk of Earth's liquid core is undergoing turbulent convection and the horizontal temperature fluctuations within the adiabatically well-mixed fluid are expected to be very small ($\mathrm{o}\{10^{-4}\mathrm{K}\}$)[1,2]. Since the thermal heterogeneity in the lowermost mantle is much stronger than in the core ($\mathrm{o}\{10^{2}\mathrm{K}\}$) and evolves much more slowly, the mantle imposes a laterally varying pattern of heat flux across the core-mantle boundary (CMB)[3,4]. Estimates of the lateral variations in CMB heat flux[5–7] are sufficiently large that significant regional variations in core dynamics are expected[8–12], particularly near the top of the core.

Seismic studies[13–15] have found body wave speeds near the top of the core that depart from those expected if the entire core is adiabatically and chemically well-mixed; although unavoidable limitations in the geographic coverage of seismic data result in under-sampling of large geographic regions of the outermost core. The seismic wave speeds have been matched to a compositional model for the core[14] and interpreted as the signature of a global layer that is both thick ($\sim$300 km) and strongly stratified (Brunt-Väisälä periods of 1.63–3.43 hr). However, other studies[16,17] have found that the seismic structure of the core does not require global stratification.

A stratified layer at the top of the core would support a range of wave dynamics not found in a fully convecting core[18]; for example, MAC waves, which involve Magnetic, Archimedean, and Coriolis forces. Assuming such a layer is present, a model of MAC waves can match the decadal axisymmetric velocity fluctuations in a core flow model[19,20], though this explanation is not unique[21]. Models that match the geomagnetic variations have a stratified layer $\sim$140 km thick with a maximum Brunt-Väisälä frequency that is roughly diurnal[19,20]; which is somewhat thinner and an order of magnitude less strongly stratified than models derived from seismic wave speeds. Global stratification would also influence the structure of the geomagnetic field[11,22]. Non-axisymmetric patches of concentrated magnetic flux at high latitudes and reversed flux in the southern Atlantic[23] are hard to explain without invoking radial motion[24] within ~ 100 km of the CMB[25], which is incompatible with models of thick global stratification.

Three principle mechanisms have been invoked to explain a global non-adiabatic structure at the top of the core. The first mechanism[26] supposes that the core has slowly cooled to a point where the heat flux, q, across the CMB has fallen below the adiabatic heat flux, q_{ad}. This scenario produces a wide range of thickness estimates[27] that rely on the poorly-known CMB heat flow and much-debated core conductivity[28]. The second mechanism invokes chemical diffusion, either along the core pressure gradient[29] or across the CMB from the mantle[30], which enriches the top of the core in light elements. The third possibility is emplacement of a light layer during core formation[31], which must then avoid disruption throughout the lifetime of the Earth or by the moon-forming impact[32]. However, all of these mechanisms are motivated by the idea of a global stable layer at the top of the core and therefore cannot explain the seismic and geomagnetic observations that are incompatible with global stratification.

We argue that the relevant scenario is not global stratification but regional thermal inversion. A net superadiabatic heat flow across the CMB ensures the bulk of the core remains vigorously convecting and adiabatically well mixed; however, sufficiently warm regions in the lowermost mantle reduce q below $q_{\rm ad}$ allowing regional accumulations of hot fluid at the top of the core. The radial temperature gradient ($\partial T/\partial r$) within the accumulated hot fluid can be insufficient to drive convection, resulting in relatively quiescent fluid volumes that we refer to as regional inversion layers. The spatial extent and buoyancy anomaly of these regional inversion layers are primarily set by the long-wavelength high-amplitude variations in CMB heat flux imposed on the core by the mantle. Large and strong regional inversion layers can dominate the spherically averaged temperature profile resulting in an apparent thermal stratification near the top of the core even though much of the core's surface remains actively convecting. This scenario allows for both substantial non-adiabatic structure at the top of the core, as has been inferred from seismology, and areas of active upwelling, as inferred from geomagnetism, thereby resolving the apparent paradox that arises in scenarios of global stratification. There is no doubt that the fundamental physical mechanism that underpins our scenario, namely large lateral variations in CMB heat flux, exists within the Earth; the only question is how significant its influence might be.

Modelling of Regional Inversion Layers

We investigate regional inversion layers in the core using a suite of numerical simulations of non-magnetic rotating convection that includes two patterns and two amplitudes of CMB heat flux heterogeneity (see methods and our previous work[12]). The amplitude of CMB heat flux heterogeneity in our numerical model is described by $q^{\star} = \frac{q_{\rm max}-q_{\rm min}}{q_{\rm ave}}$, where $q_{\rm max}$, $q_{\rm min}$, and $q_{\rm ave}$ are the maximum, minimum and horizontally averaged heat fluxes through the outer boundary, respectively. In this study we consider strong lateral variations in CMB heat flux with $q^{\star} = \{2.3, 5.0\}$. We impose one of two patterns of CMB heat flux heterogeneity. The first pattern is derived from seismic tomography[33] under the assumption that Large Low Velocity Provinces (LLVP's) are anomalously warm and therefore impose a reduced CMB heat flux on the core. The second is a hemispheric pattern that could represent the configuration of mantle flow during times of super-continent formation (for the hemispheric pattern, q_{min} is located under Null Island).

Numerical models of core convection can be characterised by three control parameters: the Prandtl number (Pr), which is the ratio of the fluid's viscous and thermal diffusivities; the Rayleigh number ($\widetilde{Ra}$) and the Ekman number (E), which primarily reflect balances between buoyancy, rotational, and viscous forces. Our simulations consider higher $\widetilde{Ra}$ and lower E than previous models that incorporate CMB heat flux heterogeneity[9–11]. In particular, we restrict our attention to simulations for which $\widetilde{Ra}$ is at least ten times greater than the critical Rayleigh number for the onset of convection ($\widetilde{Ra}_{\mathrm{c}}$) to ensure that we have left the weakly non-linear regime near the onset of convection. Consideration based on the force balance between inertia, viscosity, and rotation suggests that the dynamic regime be characterised using the Reynolds number, $Re = UL/\nu$, and Rossby number, $Ro = U/2\Omega L = ReE$, where U and L are the characteristic velocity and length scale of the flow, respectively, and ν is the magnetic diffusivity. Assuming a turbulent viscosity value for the core, our simulations are within one to two orders of magnitude of Earth-like values for these emergent parameters (Table 1); crucially, these parameters indicate that the dynamics in our simulations are both turbulent (large Re) and strongly influenced by rotation (small Ro) as in Earth's core. Our simulations produce small scale behaviour (e.g., plumes, jets; see supplementary movies) qualitatively similar to those observed in comparable laboratory experiments[34,35].

In all of our simulations we find that convectively-stable regions of thermal inversion ($\partial T/\partial r > 0$) can be maintained over large lateral and radial extents, although the bulk of the core remains strongly convecting and hence well mixed on short length scales (figures 1, 2). Even in regions where the CMB heat flux remains superadiabatic, an inversion layer can exist a few hundred kilometres below the CMB as azimuthal flow sweeps hot material horizontally. The lateral and depth extents of the regional inversion layers are associated with the long wavelengths of the imposed boundary heterogeneity rather than the small wavelengths of the convecting core fluid (figure 1, supplementary figure 1). Indeed the small scales of the convective fluctuations inhibit their ability to disrupt the large regions of thermal inversion[29,36]; previous studies at low $\widetilde{Ra}$ did not find the stratification signal[9], perhaps because the potentially stable regions were disrupted by the large scale convective patterns close to onset.

The strength of the thermal inversion is characterised by the maximum Brunt-Väisälä frequency (N), which we normalise relative to 2Ω (twice the planetary rotation rate). Scaling analysis (see methods) shows that the strength of the inversion should vary as

$$\left.\frac{N}{2\Omega}\right|_{\max} \approx \left(\frac{1}{r_{\mathrm{o}}^{\star}}\right)\sqrt{\frac{\widetilde{Ra}E}{Pr}\left(\frac{q^{\star}-2}{2}\right)}, \tag{1}$$

where $r_{\mathrm{o}}^{\star}$ is the dimensionless CMB radius. Extrapolation to the Earth must therefore account for both the increase in $\widetilde{Ra}$ and the decrease in E relative to numerical simulations (table 1). Stronger boundary heterogeneity (larger $q^{\star}$) implies more anomalous $\partial T/\partial r$ at the CMB and thus N is proportional to $q^{\star}$.

The value of $q^{\star}$ can be estimated from first-principles calculations of thermal conductivity coupled to seismic tomographic models[6] that suggest heat flux across the CMB ranges from roughly $0 - 140$ mW/m^2. Much of the net radial heat flow within the core occurs due to conduction along the adiabatic temperature gradient[28]; this contribution needs to be removed when considering the relation between our Boussinesq model and the Earth. The super-adiabatic heat flow across the CMB has been estimated as 0.6 TW based on a theoretical scaling between inertial and buoyancy forces in rotating convection[37]. These values suggest $q^\star$ for the Earth may be as large as $\sim$35, in which case $N/2\Omega \approx 2$ is predicted for the Earth for reasonable estimates of other physical parameters (supplementary table 1).

No theoretical scaling exists for the thickness of the regional inversion layers; they are not simple boundary layers, which would thin both as $\widetilde{Ra}$ is increased and as E is decreased towards Earth-like values. Instead we find a competition between thinner layers as the Ekman number is reduced but generally thicker layers as the Rayleigh number is increased for a given choice of $q^\star$ and CMB heat-flux pattern (figure 2 and supplementary figures 2 and 3).

If the regional inversion layers are sufficiently large and strong, the horizontally-averaged temperature gradient near the top of the core can become positive (figures 2, 3), an apparent global stratification despite the average heat flux across the CMB being strongly superadiabatic. Regional inversion layers that are both thick (several hundred kilometres) and strong ($N/2\Omega \approx \{10^{-2} - 10^{0}\}$) are ubiquitous in our simulations and apparent global stratification signals occur in our highest $\widetilde{Ra}$ runs. As the buoyancy forcing is increased the bulk of the core becomes more isothermal, thereby causing the horizontally averaged temperature gradient near the top of the core to be increasingly dominated by the large gradients that exist in the regional inversion layers.

Discussion

Thermal variations in Earth's lowermost mantle are sufficiently strong that large areas of the CMB are expected to have a subadiabatic heat flux. Such areas will inevitably inhibit convection in the outermost liquid core resulting in the development of horizontally extensive regional inversion layers. The strength and extent of these regions is set by the boundary heterogeneity, which is faithfully represented in our simulations; therefore, we argue that broad and thick regional inversion layers should be expected in the Earth. Following or modelling results, regional inversion layers should be most prominent in equatorial regions and particularly under the Pacific and African LLVP's. Apparent global stratification results when the regional inversions control the sign of the global average radial temperature gradient, which is particularly likely at the high Rayleigh number conditions relevant to the Earth. Seismic studies of average structure, or with an unfortunate geographic sampling, might well mistake extensive regional inversion layers for global stratification.

Unlike our Boussinesq numerical model, the anomalous regions in Earth's core need not have a strictly positive thermal gradient, they need only have a subadiabatic gradient to be dynamically distinct from the bulk of the core. The lateral temperature differences expected[1,2] within convecting regions of the outer core are very small; however, the temperature difference between actively convecting regions and the relatively stagnant regional inversion layers can be far larger because it is set by the long-wavelength and large amplitude heterogeneity in heat flux boundary conditions and not the internal convective dynamics. The temperature difference between the top of actively convecting regions and the regional inversion layers depends on the layer thickness, $q^\star$ and net superadiabatic heat flow across the CMB; assuming purely thermal convection a simple theoretical analysis suggests that the boundary-forced temperature variations can be orders of magnitude larger than those associated with the free convection (see methods, supplementary figure 4). The CMB heat flux heterogeneity will drive flows, modulated by the magnetic field[3], which previous studies[38–40] have used to explain long-term non-axisymmetric features of the geomagnetic field.

Convection in Earth's core arises due to the release of both compositional and thermal buoyancy as the core cools and the inner core solidifies. Positive correlation between temperature and composition is expected under the codensity approximation[2,11] and would result in the thermal inversion layers also being compositionally distinct from the actively convecting region. Although the core loses heat to the mantle, it is generally assumed that the light element released by inner core solidification does not escape to the mantle[2,4]. The density anomaly, and hence dynamics, of the regional inversion layers will depend on the relative contributions of thermal and compositional buoyancy within these regions.

Although radial motion would be inhibited within a strongly stratified global layer, the regional inversion layers in our simulations are dynamically connected to the rest of the core and thus radial velocity is not completely suppressed within them (figure 4). The lateral variations in CMB heat flux drive thermal winds that can sweep material from these regions into the well-mixed, vigorously convecting bulk and result in a broad, weak upwelling through the regional inversion layers. Unlike previous studies that consider subadiabatic, or weakly superadiabatic, heat flux at the CMB[11,26,27,41] all of the simulations we consider here are strongly supercritical ($\widetilde{Ra} \geq 10\widetilde{Ra}_{\mathrm{c}}$), even those for which the top of the core has an apparent global thermal stratification. In all of our simulations the bulk of the core is vigorously convecting and the regional inversion layers are not stagnant. As a result, there is no difficulty in reconciling this scenario with both geomagnetic observations that suggest upwelling near the CMB[25] and seismic observations of a relatively thick anomalous structure[14].

Fluid flow in inversion layers is different to that in the bulk of the core (figure 4), which would result in different geomagnetic variation. Observed regional patterns in geomagnetic secular variation and inferred core dynamics[42,43] might include a signature of regional inversion layers. In our model both Large Low Velocity Provinces are associated with low CMB heat flux and thus regional inversion layers; however, the latitudinal and longitudinal extents of the two LLVP's are quite different, which could result in differing influences on core thermal structure and hence geomagnetic variation. A hemispheric difference could also arise due to differences in temperature between the Pacific and African LLVP's, which might reflect differing balances between thermal and chemical contributions to these LLVP's origins.

In contrast to distinguishing between the different mechanisms proposed for inducing global stratification, the persistent regional inversion layers scenario suggested by our simulations provides a clear avenue to observational investigation. The geometry and strength of regional inversion layers in the core depends on the pattern and amplitude of the imposed heat flux heterogeneity, which is set by the distributions of both temperature and thermal conductivity in the lowermost mantle. Given suitable geographic coverage of seismic ray paths and sufficient understanding (for example, from 3D wave-propagation models) of how *SmKS* phases are influenced by regional inversion layers, it would be possible to test whether the average seismic structure at the top of the core is truly the result of global stratification or if it is instead the signature of large boundary-forced regional inversion layers.

Methods

Governing equations and parameter regime. We employ a numerical model of non-magnetic rotating convection of a homogeneous Boussinesq fluid confined within a rotating spherical shell[44], with fixed-flux thermal boundary conditions and no slip velocity boundary conditions. In non-dimensional form the conservation equations for momentum, energy, and mass are

$$\frac{E}{Pr}\left(\frac{\partial \boldsymbol{u}}{\partial t} + (\boldsymbol{u}\cdot\boldsymbol{\nabla})\,\boldsymbol{u}\right) + \hat{\boldsymbol{z}}\times\boldsymbol{u} = -\boldsymbol{\nabla}P + \widetilde{Ra}T'\boldsymbol{r} + E\nabla^2\boldsymbol{u}, \tag{2}$$

$$\frac{\partial T}{\partial t} + (\boldsymbol{u}\cdot\boldsymbol{\nabla})\,T = \nabla^2 T, \tag{3}$$

$$\boldsymbol{\nabla}\cdot\boldsymbol{u} = 0, \tag{4}$$

where $\boldsymbol{u}$ and T are the velocity and temperature fields, respectively, and T' are the temperature fluctuations relative to the steady-state temperature profile in the absence of flow. The pressure term, P, includes the centrifugal potential. The fluid is characterised by its constant thermal expansion, α, thermal diffusivity, κ, kinematic viscosity, ν, and reference density, ρ_0. The fluid shell is defined by its inner and outer boundaries, r_i and r_o, respectively, and rotates with a constant angular velocity $\mathbf{\Omega} = \Omega\hat{\boldsymbol{z}}$. Gravity varies with radius according to $\boldsymbol{g} = -(g_\mathrm{o}/r_\mathrm{o})\boldsymbol{r}$. We have non-dimensionalised using the shell thickness $L = r_\mathrm{o} - r_\mathrm{i}$ for the length scale, the thermal diffusion time $\tau = L^2/\kappa$ for the time scale, and β/L for the temperature scale, where $\beta = Q/4\pi k$, Q is the total heat flow through the outer boundary, $k = \kappa\rho_0 C_p$ is the thermal conductivity and C_p the heat capacity of the fluid. The resulting control parameters are the Prandtl number $Pr = \frac{\nu}{\kappa}$, Ekman number $E = \frac{\nu}{2\Omega L^2}$, and modified Rayleigh number $\widetilde{Ra} = \frac{\alpha g_\mathrm{o}\beta}{2\Omega\kappa}$. The amplitude of the heterogeneity in our heat flux boundary condition is measured by $q^\star = (q_\mathrm{max} - q_\mathrm{min})/q_\mathrm{ave}$, where q_max, q_min, and q_ave are the maximum, minimum and horizontally averaged heat fluxes through the outer boundary, respectively.

Our previous study[12] includes a suite of 106 simulations with values of $q^\star = \{0.0, 2.3, 5.0\}$, $Pr = 1$, $E = \{10^{-4}, 10^{-5}, 10^{-6}\}$, and $\widetilde{Ra}$ up to $\sim$800 times the critical value for the onset of convection $\widetilde{Ra}_\mathrm{c}$. The critical Rayleigh number increases as the Ekman number is reduced and has values of $\widetilde{Ra}_\mathrm{c} = \{16.4, 24.7, 41.0\}$ for the three values of E that we use. Here we include six additional simulations with the hemispheric boundary forcing and $E = 10^{-6}$. In this study we do not include results from our simulations that have homogeneous CMB boundary heat flux ($q^\star = 0.0$) or that are only weakly super-critical ($\widetilde{Ra} < 10\widetilde{Ra}_\mathrm{c}$), leaving a total of 68 simulations.

The pattern and amplitude of CMB heat flux variations are difficult to estimate because they must be inferred from seismic tomography accounting for possible compositional effects and phase changes in the lower mantle. Nevertheless, several studies[5–7] have found a minimum heat flux of $q_\mathrm{min} \approx 0$ mW m^{-2}, while the maximum heat flux q_max could rise above 200 mW m^{-2}. The adiabatic gradient at the CMB is $\partial T_\mathrm{ad}/\partial r = g\gamma T/\phi \approx -0.875 \pm 0.125$ K km^{-1} with the seismic parameter ϕ and gravity g taken from PREM[45] and the Grüneisen parameter $\gamma = 1.3 - 1.5$ spanning the available estimates[46]. Using low[47] and high[28] thermal conductivity values gives $q_{\mathrm{ad}} = -k\partial T_{\mathrm{ad}}/\partial r = 15 - 100$ mW m^{-2} and therefore hot regions of the lower mantle will result in a subadiabatic heat flux across the CMB. The relative strength of CMB anomalies is often measured by the parameter $q^\star = (q_{\max} - q_{\min})/(q - q_{\mathrm{ad}})$, which can take either sign given estimates[48] of $q = 30 - 110$ mW m^{-2}. Here we are interested in the case $q^\star > 0$, as $q^\star$ of at least $o\{1\}$ is expected within the Earth[6] and it could be significantly greater (indeed $q^\star$ is unbounded as $q \to q_{\mathrm{ad}}$). If $q^\star$ is large, as expected for the Earth, thermal boundary forcing should exert a significant influence on core convection[34,35].

Brunt-Väisälä frequency. The frequency of oscillation of a radially displaced fluid parcel within a layer having stable density stratification ($\partial\rho/\partial r < 0$) is known as the buoyancy or Brunt-Väisälä frequency and is defined by

$$N = \sqrt{-\frac{g}{\rho_0}\frac{\partial \rho}{\partial r}} = \sqrt{g\alpha\frac{\partial T}{\partial r}}, \tag{5}$$

if the density anomalies arise due to purely thermal effects. Non-dimensionalising frequency by 2Ω, in combination with our temperature and distance scalings gives

$$\frac{N}{2\Omega} = \sqrt{\frac{g\alpha\beta}{4\Omega^2 L^2}\frac{\partial T^\star}{\partial r^\star}} = \sqrt{\frac{\widetilde{Ra}E}{Pr}\frac{\partial T^\star}{\partial r^\star}}, \tag{6}$$

where $T^\star$ and $r^\star$ are non-dimensional temperature and radius, respectively.

The steepest temperature gradient within a regional inversion layer corresponds to the maximum buoyancy frequency and we expect that the steepest gradient near the top of the core is close to that set by $q_{\min}$ of the imposed CMB heat flux. However, along some radial profiles (for example, Africa, figure 2) the maximum of dT/dr occurs some depth below the CMB. A simple pattern of heat flux heterogeneity would have $q_{\mathrm{ave}} = (q_{\mathrm{max}} + q_{\mathrm{min}})/2$ and from the definition of our boundary conditions $q_{\mathrm{ave}} = k\beta/r_{\mathrm{o}}^2$; therefore we expect

$$\left.\frac{N}{2\Omega}\right|_{\mathrm{max}} \approx \left(\frac{1}{r_{\mathrm{o}}^{\star}}\right)\sqrt{\frac{\widetilde{Ra}E}{Pr}\left(\frac{q^{\star}-2}{2}\right)}. \tag{7}$$

Boundary-forced lateral temperature variations In a fully convecting core an adiabatic temperature gradient ($\partial T_{\mathrm{ad}}/\partial r$) will extend from the ICB to the CMB, except within thin boundary layers. Within a regional inversion layer a shallower conductive profile ($\partial T_{\mathrm{c}}/\partial r$) will exist. The temperature difference at the CMB between a fully convecting region and the top of a regional inversion layer of thickness h will be approximately

$$\delta T \approx h\left(\partial T_{\mathrm{ad}}/\partial r - \partial T_{\mathrm{c}}/\partial r\right). \tag{8}$$

Setting the conductive temperature gradient throughout the inversion layer equal to the minimum CMB heat flux gives

$$\delta T \approx \frac{h}{k}\left(q_{\mathrm{ad}} - q_{\mathrm{min}}\right), \tag{9}$$

where k is the thermal conductivity of the core.

To estimate δT for the Earth, we use $q^{\star} = (q_{\mathrm{max}} - q_{\mathrm{min}})/(q - q_{\mathrm{ad}})$ and $q - q_{\mathrm{ad}} = Q_{\mathrm{conv}}/4\pi r_{\mathrm{o}}^2$ to rewrite equation (9) as

$$\delta T \approx \frac{hQ_{\mathrm{conv}}}{4\pi r_{\mathrm{o}}^2 k}\left(0.5q^{\star} - 1\right). \tag{10}$$

The thickness of the regional inversion layers arises dynamically in our models and depends on both $q^{\star}$ and Q_{conv}. Here we assume a superadiabatic heat flow of $Q_{\mathrm{conv}} = 0.6$ TW and a thermal conductivity $k = 100$ W m^{-1} K^{-1} and simply vary $q^\star$ and h to estimate the temperature difference at the CMB between fully convecting and subadiabatic regions. The likely values of δT are generally on the order of 10's of kelvin (supplementary figure 4). The largest values corresponding to particularly thick layers that will have a large Brunt-Väisälä frequency. To explain a layer with $N \approx \Omega$ by purely thermal effects requires $\partial T/\partial r \approx 35$ mK/km, with the temperature gradient scaling as N^2. Any compositional contribution would reduce the required temperature gradient for a given buoyancy frequency.

1. Roberts, P. H. & Aurnou, J. M. On the theory of core-mantle coupling. *Geophysical & Astrophysical Fluid Dynamics* **106**, 157–230 (2012).

2. Jones, C. A. Thermal and Compositional Convection in the Outer Core. In Olson, P. (ed.) *Core Dynamics*, 115–159 (Elsevier, Amsterdam, 2015).

3. Lister, J. R. Thermal winds forced by inhomogeneous boundary conditions in rotating, stratified, hydromagnetic fluid. *Journal of Fluid Mechanics* **505**, 163–178 (2004).

4. Olson, P. Thermal interaction of the core and mantle. In *Earth's Core and Lower Mantle*, 1–38 (Taylor & Francis, New York, 2003).

5. Nakagawa, T. & Tackley, P. J. Lateral variations in CMB heat flux and deep mantle seismic velocity caused by a thermal–chemical-phase boundary layer in 3D spherical convection. *Earth and Planetary Science Letters* **271**, 348–358 (2008).

6. Stackhouse, S., Stixrude, L. & Karki, B. B. First-principles calculations of the lattice thermal conductivity of the lower mantle. *Earth and Planetary Science Letters* **427**, 11–17 (2015).

7. Olson, P., Deguen, R., Rudolph, M. L. & Zhong, S. Core evolution driven by mantle global circulation. *Physics of the Earth and Planetary Interiors* **243**, 44–55 (2015).

8. Gibbons, S. J., Gubbins, D. & Zhang, K. Convection in rotating spherical fluid shells with inhomogeneous heat flux at the outer boundary. *Geophysical & Astrophysical Fluid Dynamics* **101**, 347–370 (2007).

9. Davies, C. J., Gubbins, D. & Jimack, P. K. Convection in a rapidly rotating spherical shell with an imposed laterally varying thermal boundary condition. *Journal of Fluid Mechanics* **641**, 335–358 (2009).

10. Dietrich, W., Hori, K. & Wicht, J. Core flows and heat transfer induced by inhomogeneous cooling with sub- and supercritical convection. *Physics of the Earth and Planetary Interiors* **251**, 36–51 (2016).

11. Olson, P., Landeau, M. & Reynolds, E. Dynamo tests for stratification below the core-mantle boundary. *Physics of the Earth and Planetary Interiors* **271**, 1–18 (2017).

12. Mound, J. E. & Davies, C. J. Heat transfer in rapidly rotating convection with heterogeneous thermal boundary conditions. *Journal of Fluid Mechanics* **828**, 601–629 (2017).

13. Lay, T. & Young, C. J. The stably-stratified outermost core revisited. *Geophysical Research Letters* **17**, 2001–2004 (1990).

14. Helffrich, G. & Kaneshima, S. Outer-core compositional stratification from observed core wave speed profiles. *Nature* **468**, 807–810 (2010).

15. Kaneshima, S. Array analyses of SmKS waves and the stratification of Earth's outermost core. *Physics of the Earth and Planetary Interiors* **276**, 234–246 (2018).

16. Alexandrakis, C. & Eaton, D. W. Precise seismic-wave velocity atop Earth's core: No evidence for outer-core stratification. *Physics of the Earth and Planetary Interiors* **180**, 59–65 (2010).

17. Irving, J. C. E., Cottaar, S. & Lekić, V. Seismically determined elastic parameters for Earth's outer core. *Science Advances* **4**, 1–9 (2018).

18. Braginsky, S. I. Dynamics of the stably stratified ocean at the top of the core. *Physics of the Earth and Planetary Interiors* **111**, 21–34 (1999).

19. Buffett, B. Geomagnetic fluctuations reveal stable stratification at the top of the Earth's core. *Nature* **507**, 484–487 (2014).

20. Buffett, B., Knezek, N. & Holme, R. Evidence for MAC waves at the top of Earth's core and implications for variations in length of day. *Geophysical Journal International* **204**, 1789–1800 (2016).

21. Buffett, B. A., Mound, J. & Jackson, A. Inversion of torsional oscillations for the structure and dynamics of Earth's core. *Geophysical Journal International* **177**, 878–890 (2009).

22. Christensen, U. R. & Wicht, J. Models of magnetic field generation in partly stable planetary cores: Applications to Mercury and Saturn. *Icarus* **196**, 16–34 (2008).

23. Olsen, N. *et al.* The CHAOS-4 geomagnetic field model. *Geophysical Journal International* **197**, 815–827 (2014).

24. Amit, H. Can downwelling at the top of the Earth's core be detected in the geomagnetic secular variation? *Physics of the Earth and Planetary Interiors* **229**, 110–121 (2014).

25. Gubbins, D. Geomagnetic constraints on stratification at the top of Earth's core. *Earth, Planets and Space* **59**, 661–664 (2007).

26. Lister, J. R. & Buffett, B. A. Stratification of the outer core at the core-mantle boundary. *Physics of the Earth and Planetary Interiors* **105**, 5–19 (1998).

27. Gubbins, D., Alfè, D., Davies, C. & Pozzo, M. On core convection and the geodynamo: Effects of high electrical and thermal conductivity. *Physics of the Earth and Planetary Interiors* **247**, 56–64 (2015).

28. Davies, C., Pozzo, M., Gubbins, D. & Alfè, D. Constraints from material properties on the dynamics and evolution of Earth's core. *Nature Geoscience* **8**, 678–685 (2015).

29. Gubbins, D. & Davies, C. J. The stratified layer at the core-mantle boundary caused by barodiffusion of oxygen, sulphur and silicon. *Physics of the Earth and Planetary Interiors* **215**, 21–28 (2013).

30. Buffett, B. A. & Seagle, C. T. Stratification of the top of the core due to chemical interactions with the mantle. *Journal of Geophysical Research* **115**, B04407 (2010).

31. Landeau, M., Olson, P., Deguen, R. & Hirsh, B. H. Core merging and stratification following giant impact. *Nature Geoscience* **9**, 786–789 (2016).

32. Jacobson, S. A., Rubie, D. C., Hernlund, J., Morbidelli, A. & Nakajima, M. Formation, stratification, and mixing of the cores of Earth and Venus. *Earth and Planetary Science Letters* **474**, 375–386 (2017).

33. Masters, G., Johnson, S., Laske, G. & Bolton, H. A shear-velocity model of the mantle. *Philosophical Transactions of the Royal Society A: Mathematical, Physical and Engineering Sciences* **354**, 1385–1411 (1996).

34. Sumita, I. & Olson, P. A laboratory model for convection in Earth's core driven by a thermally heterogeneous mantle. *Science* **286**, 1547–1549 (1999).

35. Sumita, I. & Olson, P. Rotating thermal convection experiments in a hemispherical shell with heterogeneous boundary heat flux: Implications for the Earth's core. *Journal of Geophysical Research* **107**, 2169 (2002).

36. Calkins, M. A. *et al.* The asymptotic equivalence of fixed heat flux and fixed temperature thermal boundary conditions for rapidly rotating convection. *Journal of Fluid Mechanics* **784**, R2 (2015).

37. Jones, C. A. Planetary magnetic fields and fluid dynamos. *Annual Review of Fluid Mechanics* **43**, 583–614 (2011).

38. Olson, P. & Christensen, U. R. The time-averaged magnetic field in numerical dynamos with non-uniform boundary heat flow. *Geophysical Journal International* **151**, 809–823 (2002).

39. Gubbins, D., Willis, A. P. & Sreenivasan, B. Correlation of Earth's magnetic field with lower mantle thermal and seismic structure. *Physics of the Earth and Planetary Interiors* **162**, 256–260 (2007).

40. Aubert, J., Finlay, C. C. & Fournier, A. Bottom-up control of geomagnetic secular variation by the Earth's inner core. *Nature* **502**, 219–223 (2013).

41. Sahoo, S., Sreenivasan, B. & Amit, H. Dynamos driven by weak thermal convection and heterogeneous outer boundary heat flux. *Physics of the Earth and Planetary Interiors* **250**, 35–45 (2016).

42. Finlay, C. C., Olsen, N., Kotsiaros, S., Gillet, N. & Tøffner-Clausen, L. Recent geomagnetic secular variation from Swarm and ground observatories as estimated in the CHAOS-6 geomagnetic field model. *Earth, Planets and Space* **68**, 112 (2016).

43. Barrois, O., Hammer, M. D., Finlay, C. C., Martin, Y. & Gillet, N. Assimilation of ground and satellite magnetic measurements: inference of core surface magnetic and velocity field changes. *Geophysical Journal International* **215**, 695–712 (2018).

44. Willis, A. P., Sreenivasan, B. & Gubbins, D. Thermal core–mantle interaction: Exploring regimes for 'locked' dynamo action. *Physics of the Earth and Planetary Interiors* **165**, 83–92 (2007).

45. Dziewonski, A. M. & Anderson, D. L. Preliminary reference Earth model. *Physics of the Earth and Planetary Interiors* **25**, 297–356 (1981).

46. Ichikawa, H., Tsuchiya, T. & Tange, Y. The P-V-T equation of state and thermodynamic properties of liquid iron. *Journal of Geophysical Research* **119**, 240–252 (2014).

47. Konôpková, Z., McWilliams, R. S., Gómez-Pérez, N. & Goncharov, A. F. Direct measurement of thermal conductivity in solid iron at planetary core conditions . *Nature* **534**, 99–101 (2016).

48. Nimmo, F. Energetics of the Core. In Olson, P. (ed.) *Core Dynamics*, 27–55 (Elsevier, Amsterdam, 2015).

49. Childs, H. *et al.* VisIt: An end-user tool for visualizing and analyzing very large data. In Bethel, E. W., Childs, H. & Hansen, C. (eds.) *High Performance Visualization*, 357–372 (Chapman and Hall, 2012).

50. Hunter, J. D. Matplotlib: A 2D graphics environment. *Computing in Science and Engineering* **9**, 90–95 (2007).

51. Waskom, M. *et al.* mwaskom/seaborn: v0.8.0 (2017).

Acknowledgements CD is supported by a Natural Environment Research Council Independent Research Fellowship (NE/L011328/1). This work used the ARCHER UK National Supercomputing Service (http://www.archer.ac.uk) and ARC2, part of the High Performance Computing facilities at the University of Leeds, UK. Figures were produced using VisIt[49], Matplotlib[50] and seaborn[51].

Competing Interests The authors declare that they have no competing financial interests.

Author Contributions All discussed and developed the central ideas and contributed to the writing of the manuscript. JM and CD carried out the numerical modelling and analysis.

Quantity	Definition	Molecular	Turbulent	Simulations
Rayleigh	$\widetilde{Ra} = \frac{\alpha g_o \beta}{2\Omega\kappa}$	4×10^{13}	2×10^{10}	$225 - 18000$
Ekman	$E = \frac{\nu}{2\Omega L^2}$	7×10^{-16}	4×10^{-11}	$10^{-6} - 10^{-4}$
Prandtl	$Pr = \frac{\nu}{\kappa}$	0.04	1	1
Reynolds	$Re = UL/\nu$	2×10^{9}	4×10^{4}	$O(10^1 - 10^3)$
Rossby	$Ro = U/2\Omega L = ReE$	1.5×10^{-6}	1.5×10^{-6}	$O(10^{-4} - 10^{-1})$

Table 1: Nondimensional numbers.

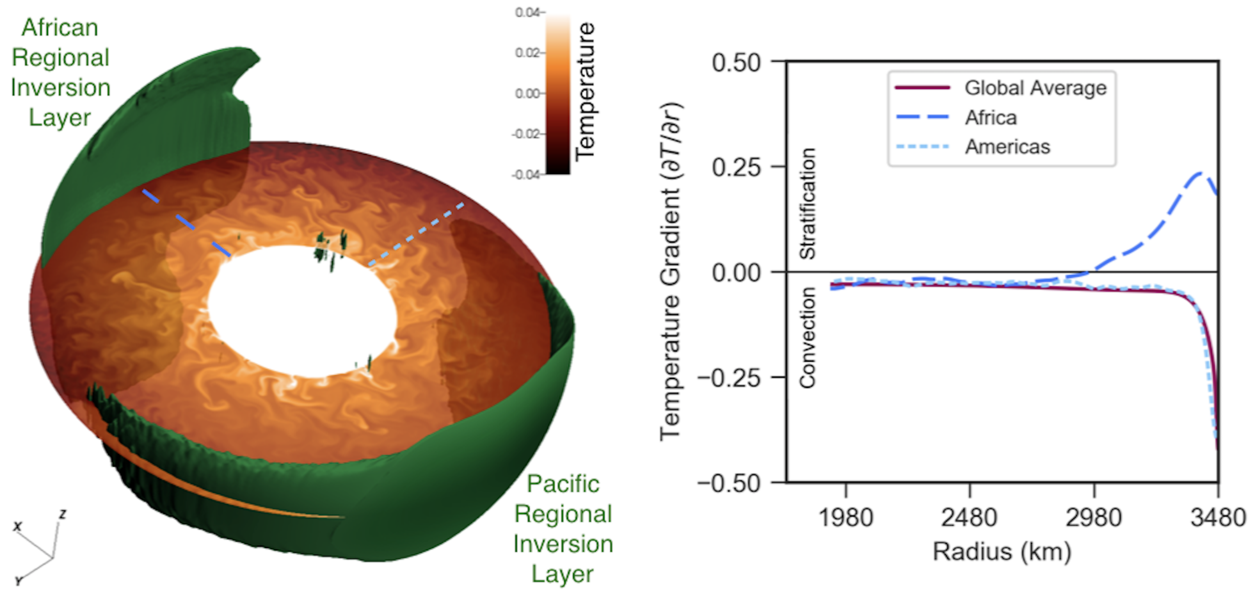

Figure 1: Thermal structure in the simulation with a tomographic CMB heat flux pattern, $q^\star = 5.0$, $E = 10^{-6}$, and $\widetilde{Ra} = 1.8 \times 10^4$. Left: Green isovolumes denote the thermally stratified regional inversion layers ($\partial T/\partial r > 0$ in the time-average); equatorial slice shows instantaneous temperature anomalies at one point in time. Right: Time-averaged profiles of radial temperature gradient ($\partial T/\partial r$) in the top half of the core ($r_\mathrm{o}/2 < r < r_\mathrm{o}$). Regional profiles on the equator ($\theta = \pi/2$) are shown for longitudes associated with Africa ($\phi = 0$, long-dash blue line) and the Americas ($\phi = 3\pi/2$, short-dash light blue line). The horizontally-averaged profile is shown by the solid magenta line. Temperature has been non-dimensionalised as described in the methods section.

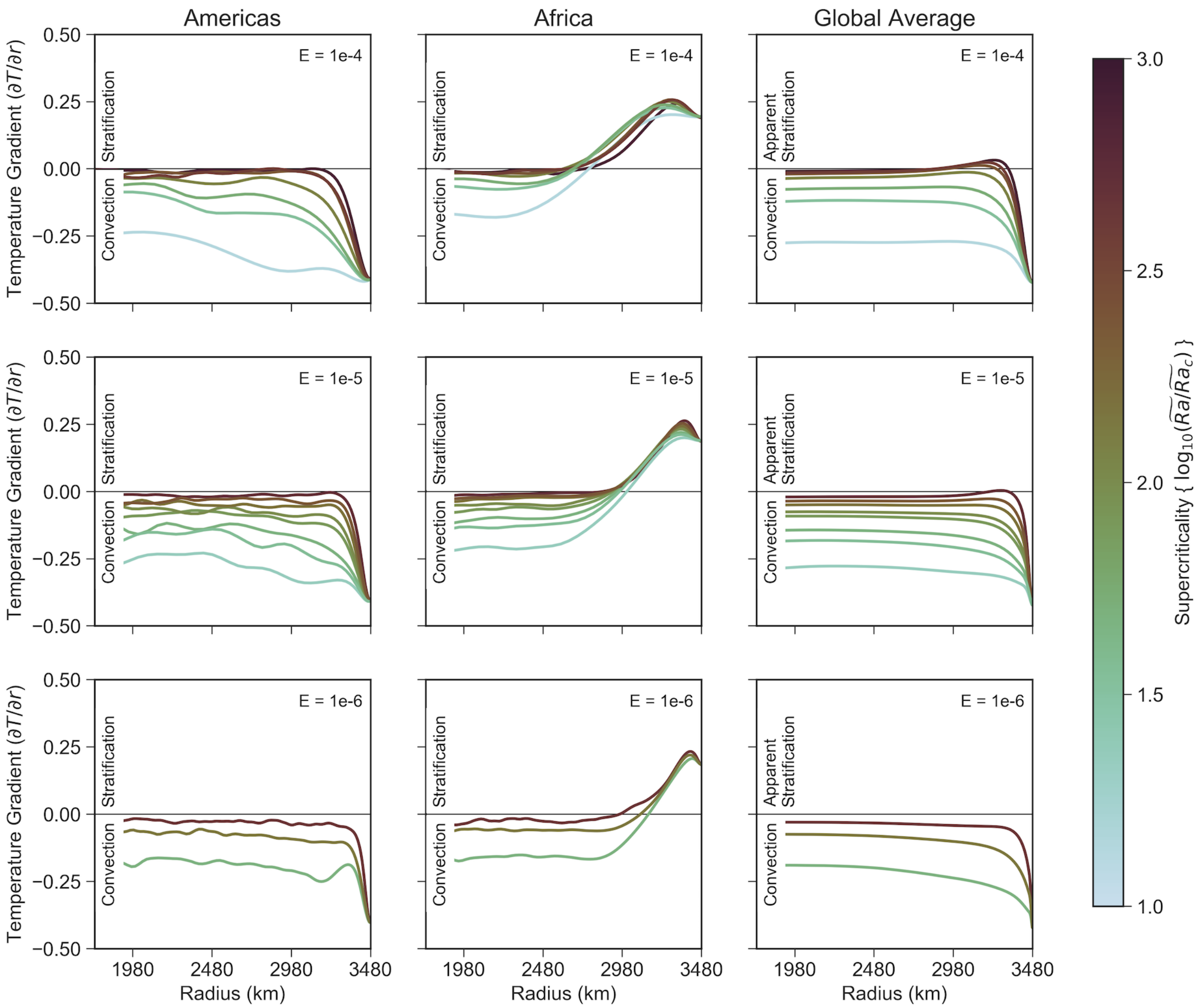

Figure 2: Profiles of time-averaged radial temperature gradient ($\partial T/\partial r$) in the top half of the core ($r_\mathrm{o}/2 < r < r_\mathrm{o}$). As in figure 1, we consider equatorial profiles under the Americas (left) and Africa (middle), as well as the global average (right). Simulations have a tomographic CMB heat-flux pattern, with $q^\star = 5.0$, and $E = 10^{-4}$ (top), 10^{-5} (middle), or 10^{-6} (bottom). Colour of the lines indicates the super-criticality of the modified Rayleigh number from 10 times critical (light) to 1000 times critical (dark). Temperature has been non-dimensionalised as described in the methods section.

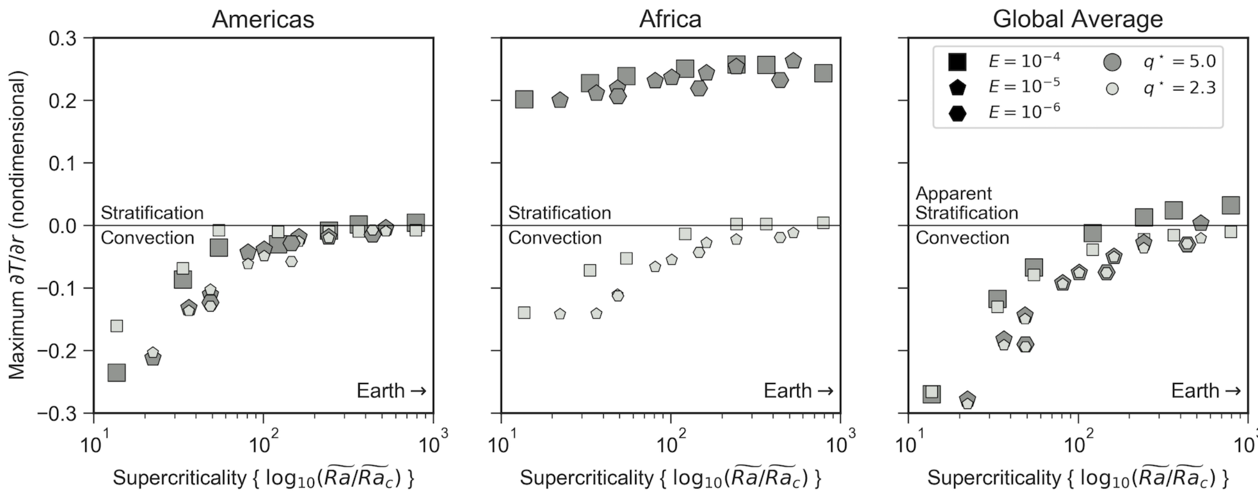

Figure 3: Maximum time-averaged radial temperature gradient ($\partial T/\partial r$) as a function of supercriticality. As in figure 2, we consider equatorial profiles under the Americas (left) and Africa (middle), as well as the global average (right). Symbol shape indicates $E = 10^{-4}$ (square), 10^{-5} (pentagon), or 10^{-6} (hexagon). Simulations have a tomographic pattern of CMB heat flux; symbol size and colour indicates $q^\star = 2.3$ (small, light grey), or 5.0 (large, grey). Temperature has been non-dimensionalised as described in the methods section.

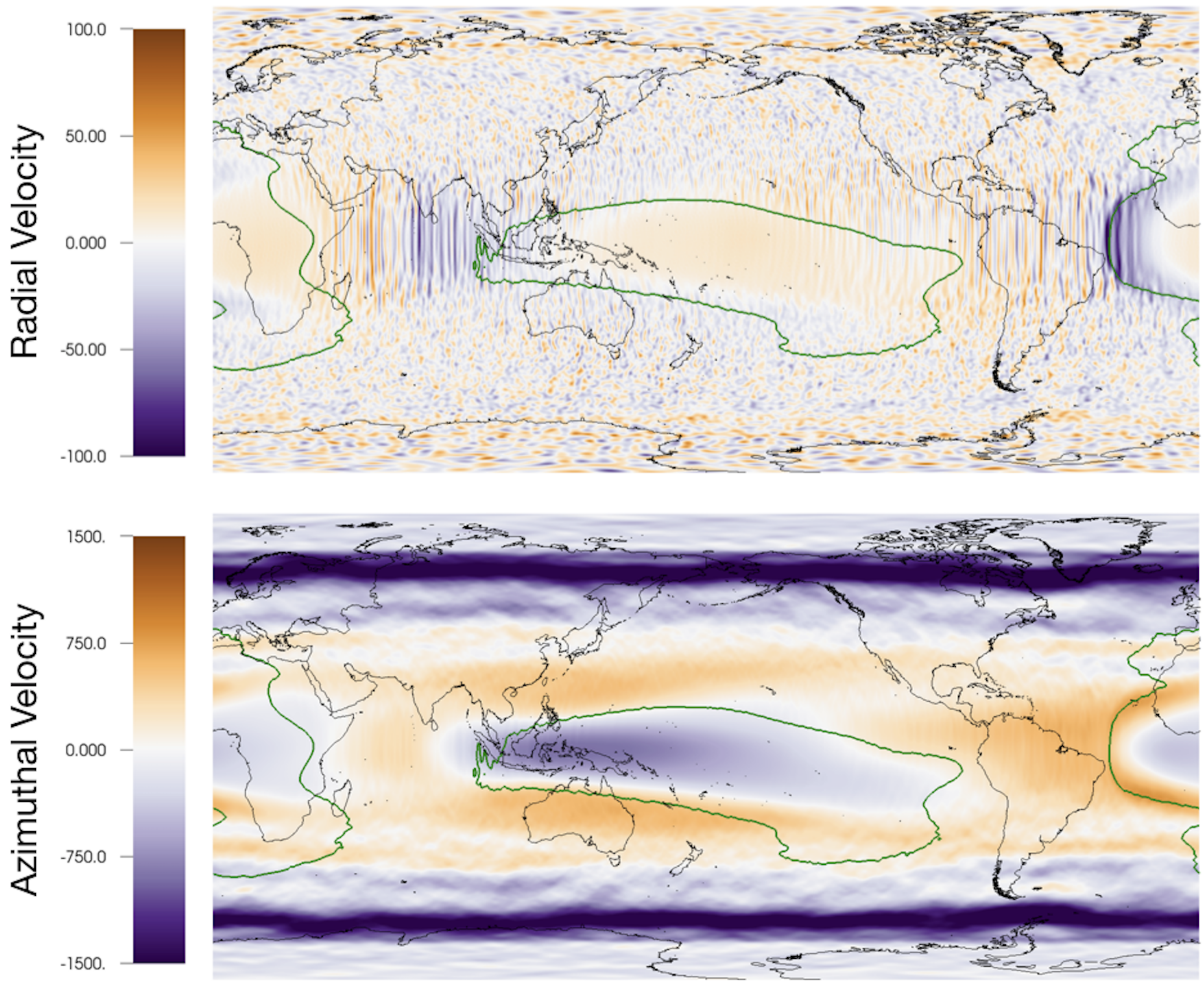

Figure 4: Flow near the top of the core for the simulation in figure 1. Time average of the radial velocity (top) and azimuthal velocity (bottom) at a depth of $\sim$100 km below the CMB. The green line denotes the boundary of the regional inversion layer ($\partial T/\partial r = 0$ contour). This is the simulation with a tomographic CMB heat flux pattern, $q^\star = 5.0$, $E = 10^{-6}$, and $\widetilde{Ra} = 1.8 \times 10^4$. The averaging was done over 37 advection times. The flow velocity is non-dimensionalised as described in the methods section.

Supplementary Information for “The Apparent Stratification at the Top of Earth’s Liquid Core”

Jon Mound[1], Chris Davies[1], Sebastian Rost[1] & Jon Aurnou[2]

[1]*School of Earth and Environment, University of Leeds, Leeds LS2 9JT, UK*

[2]*Department of Earth and Space Sciences, University of California, Los Angeles, California 90095-1567, USA.*

Supplemental Movie 1: Equatorial slices (viewed from above, Pacific to left, Africa to right) of thermal structure in the simulation with a tomographic pattern of CMB heat flux presented in figure 1 of the main text. Left: temperature field. Right: radial gradient of temperature. The movie spans approximately 2.6 advection time units, which is approximately 7% of the total model run.

Supplemental Movie 2: Equatorial slices (viewed from above, Pacific to left, Africa to right) of thermal structure in the simulation with a hemispheric pattern of CMB heat flux presented in supplemental figure 1. Left: temperature field. Right: radial gradient of temperature. The movie spans approximately 2.7 advection time units, which is approximately 7% of the total model run.

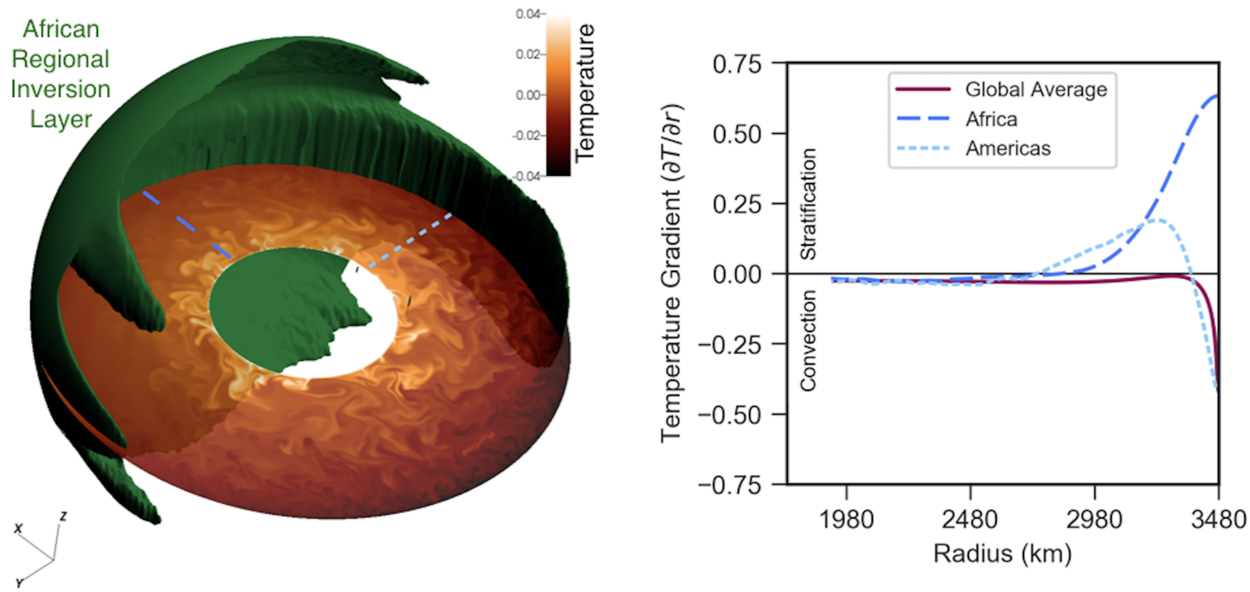

Figure 1: Thermal structure in the simulation with a hemispheric CMB heat flux pattern, $q^\star = 5.0$, $E = 10^{-6}$, and $\widetilde{Ra} = 1.8 \times 10^4$. Left: Green isovolumes denote the thermally stratified regional inversion layers ($\partial T/\partial r > 0$ in the time-average); equatorial slice shows instantaneous temperature anomalies at one point in time. Right: Time-averaged profiles of temperature gradient ($\partial T/\partial r$) in the top half of the core ($r_\mathrm{o}/2 < r < r_\mathrm{o}$). Regional profiles on the equator ($\theta = \pi/2$) are shown for longitudes associated with Africa ($\phi = 0$, long-dash blue line) and the Americas ($\phi = 3\pi/2$, short-dash light blue line). The horizontally-averaged profile is shown by the solid magenta line. Temperature has been non-dimensionalised as described in the methods section.

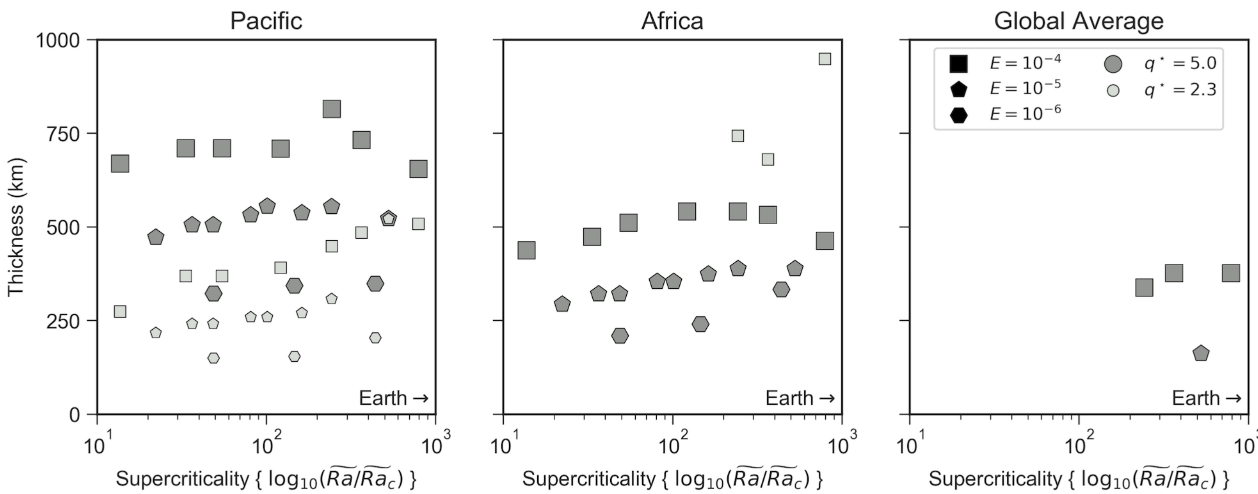

Figure 2: Thickness of the regional inversion layers under the Pacific and Africa, and the thickness of the apparent global stratification, as a function of super-criticality from all simulations with the tomographic CMB heat-flux pattern. Symbol size and colour indicates $q^\star = 2.3$ (small, light grey), or 5.0 (large, grey). Symbol shape indicates $E = 10^{-4}$ (square), 10^{-5} (pentagon), or 10^{-6} (hexagon).

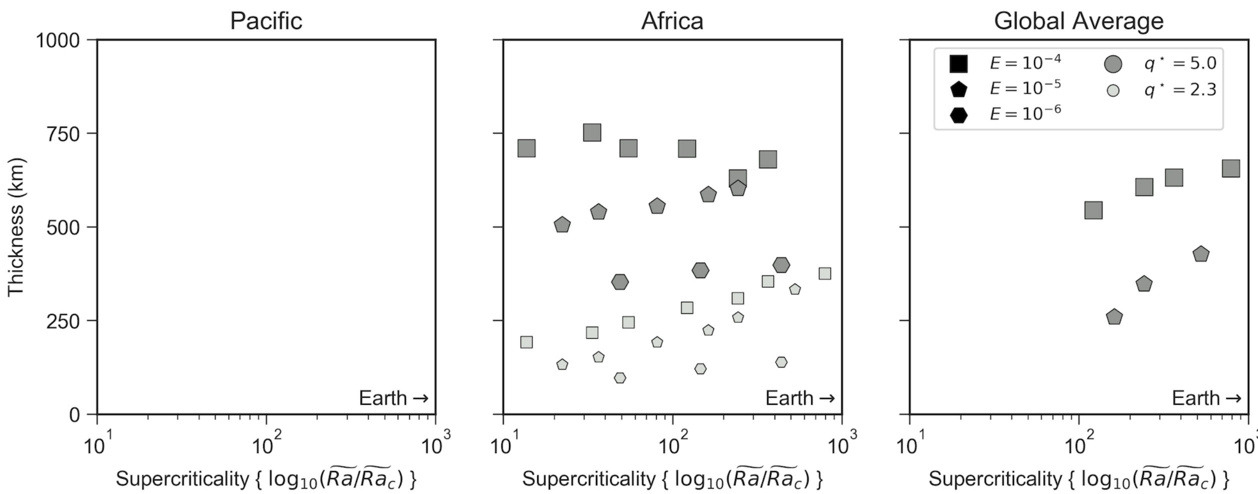

Figure 3: Thickness of the regional inversion layers under the Pacific and Africa, and the thickness of the apparent global stratification, as a function of super-criticality from all simulations with the hemispheric CMB heat-flux pattern (for this pattern no regional inversion layer forms under the Pacific). Symbol size and colour indicates $q^\star = 2.3$ (small, light grey), or 5.0 (large, grey). Symbol shape indicates $E = 10^{-4}$ (square), 10^{-5} (pentagon), or 10^{-6} (hexagon).

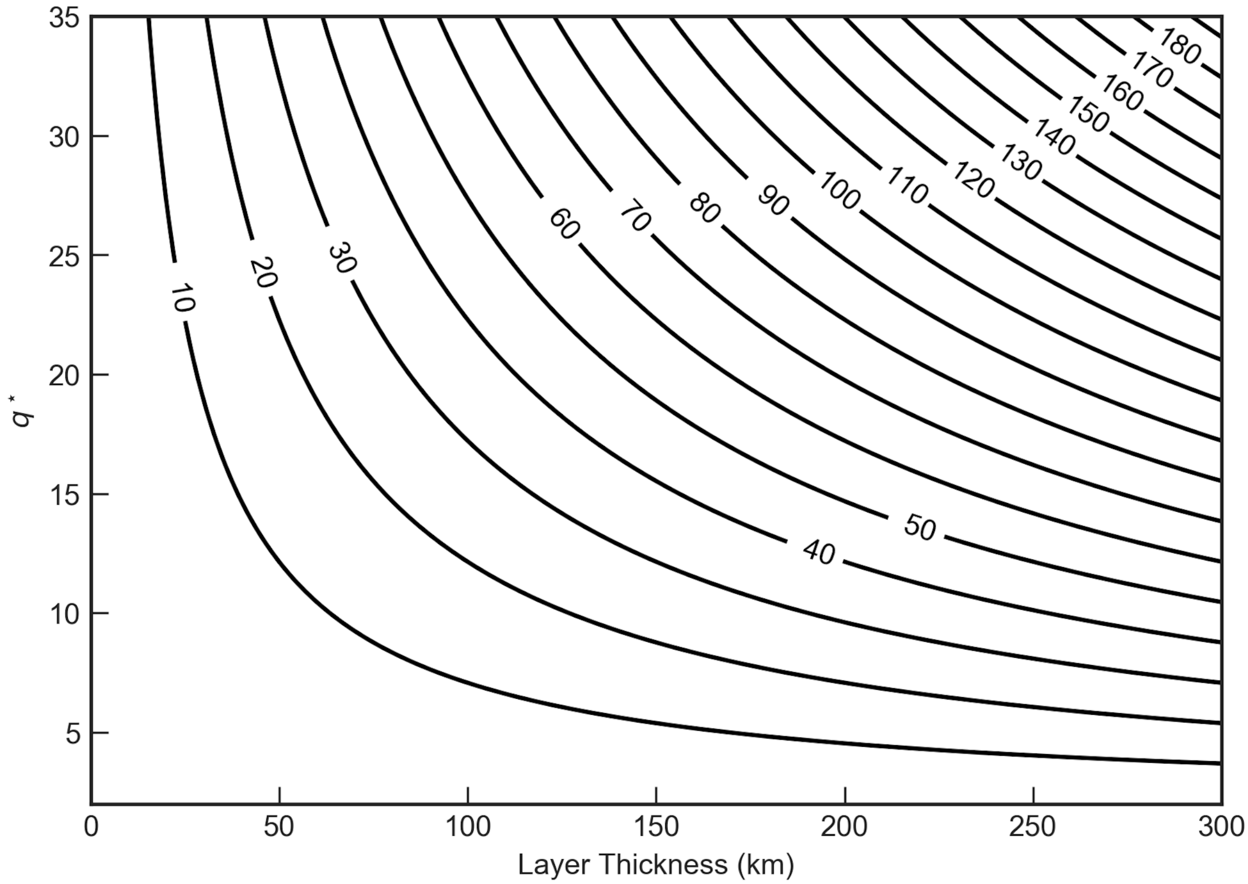

Figure 4: Excess temperature of the stratified regions. Contours of excess temperature (in kelvin) at the top of the core as a function of the layer thickness and the strength of heterogeneity, $q^\star$. This example considers a total superadiabatic heat flow across the CMB of $Q_{\rm conv} = 0.6$ TW, and thermal conductivity $k = 100$ W m^{-1} K^{-1}.

Quantity	Sybol	Value
CMB radius	r_o	3.48×10^6 m
ICB radius	r_i	1.22×10^6 m
shell thickness	$L = r_o - r_i$	2.26×10^6 m
gravitational acceleration at CMB	g_o	10 m s^{-2}
thermal expansivity	α	1.5×10^{-5} K^{-1}
rotation rate	Ω	7.29×10^{-5} s^{-1}
thermal diffusivity, molecular	$\kappa_{\rm m}$	1.3×10^{-5} m^2 s^{-1}
thermal diffusivity, turbulent	$\kappa_{\rm t}$	3×10^{-2} m^2 s^{-1}
kinematic viscosity, molecular	$\nu_{\rm m}$	5×10^{-7} m^2 s^{-1}
kinematic viscosity, turbulent	$\nu_{\rm t}$	3×10^{-2} m^2 s^{-1}
CMB superadiabatic heat flow	$Q_{\rm conv}$	0.6 TW
thermal conductivity	k	100 W m^{-1} K^{-1}
thermal forcing	$\beta = Q_{\rm conv}/(4\pi k)$	5×10^8 K m
characteristic flow speed	U	5×10^{-4} m s^{-1}

Table 1: Physical parameters.